Middle East Respiratory Syndrome Coronavirus (MERS-CoV) Infection: Chest CT Findings

Amr M. Ajlan[1]
Rayan A. Ahyad[2]
Lamia Ghazi Jamjoom[1]
Ahmed Alharthy[3]
Tariq A. Madani[4]

OBJECTIVE. The purpose of this study was to describe the chest CT findings in seven patients with Middle East respiratory syndrome coronavirus (MERS-CoV) infection.

CONCLUSION. The most common CT finding in hospitalized patients with MERS-CoV infection is that of bilateral predominantly subpleural and basilar airspace changes, with more extensive ground-glass opacities than consolidation. The subpleural and peribronchovascular predilection of the abnormalities is suggestive of an organizing pneumonia pattern.

Keywords: coronavirus, CT, high-resolution CT, Middle Eastern respiratory syndrome (MERS), Middle Eastern respiratory syndrome coronavirus (MERS-CoV), organizing pneumonia

DOI:10.2214/AJR.14.13021

Received April 19, 2014; accepted after revision May 17, 2014.

[1]Cardiothoracic Imaging Unit, Department of Radiology, King Abdulaziz University Hospital, King Abdulaziz University, Jeddah, Western Region, Saudi Arabia. Address correspondence to A. M. Ajlan (amrajlan@yahoo.com).

[2]Department of Radiology, King Faisal Specialist Hospital and Research Center, Jeddah, Western Region, Saudi Arabia.

[3]Department of Radiology, King Abdulaziz University Hospital, King Abdulaziz University, Jeddah, Western Region, Saudi Arabia.

[4]Department of Medicine, King Abdulaziz University Hospital, King Abdulaziz University, Jeddah, Western Region, Saudi Arabia.

AJR 2014; 203:782–787

0361–803X/14/2034–782

In September 2012, the acute viral respiratory disease known as Middle East respiratory syndrome (MERS) was first reported in Saudi Arabia [1]. MERS is caused by a novel virus currently named MERS coronavirus (MERS-CoV) [1, 2]. Since then, cases of MERS have been identified in Jordan, Qatar, the United Arab Emirates, Kuwait, Oman, Tunisia, Germany, France, the United Kingdom, and Italy [3]. In April 2014, an increase in the number of MERS-CoV cases in Saudi Arabia and the United Arab Emirates was reported to the World Health Organization (WHO) [4]. New cases have been recently reported in Yemen, Egypt, Greece, Malaysia, the Philippines, and the United States [5]. A history of recent travel from Saudi Arabia or the United Arab Emirates was documented in all cases recently reported outside the Middle East. As of May 9, 2014, 536 laboratory-confirmed cases have been reported to the WHO, and 145 of these patients have died [5].

Proven cases of MERS-CoV have been acquired both in the community and health care settings [2, 6, 7]. The source of MERS-CoV is not yet clear, but the origin of the infection has been linked to camels [8, 9]. An association with bats has been proposed as well [10]. Although not clearly documented in all cases, most patients acquire the illness through person-to-person transmission [2, 11]. The clinical presentation of MERS varies from mild to severe, but most reported patients developed severe illness, resulting in a high case-fatality rate [2]. MERS-CoV has been detected in previously healthy patients and patients with known comorbidities, with a larger number of reported cases in the latter group [2]. Patients with hypertension, diabetes, cardiomyopathy, chronic renal failure, malignancy, and decreased immunity appear to be at a higher risk of developing severe disease. Presenting symptoms include fever, cough, chills, dyspnea, myalgia, abdominal pain, nausea, vomiting, and diarrhea [1, 2, 6, 11]. Laboratory abnormalities that have been encountered with MERS include thrombocytopenia, lymphopenia, leukopenia, elevated serum lactate dehydrogenase (LDH), elevated aspartate aminotransferase (AST), elevated alanine aminotransferase (ALT), and abnormal renal function tests [2, 6, 7, 11]. Superinfection from viral or bacterial causes has been found in some patients and may complicate the course of the disease [11]. Severe cases of MERS may require intensive care and mechanical ventilation, with a relatively large number of patients progressing to respiratory or renal failure [1, 2, 7, 11, 12]. To our knowledge, no vaccine or specific antiviral agents are currently available against MERS-CoV [11, 12].

Despite a number of recent publications on MERS, the description of the imaging features of this disease is sparse and limited to nonimaging medical literature [2, 12]. Both airspace and interstitial opacities have been described on chest radiographs of MERS. Radiographic findings may be subtle or extensive, unilateral or bilateral, and focal or diffuse. The airspace opacities have

been nonspecific, described as focal, segmental, lobar, patchy, nodular, or confluent, whereas the interstitial changes have been described as reticular or reticulonodular. Total lung opacification and thickening of the bronchovascular markings have been reported as well. Chest CT findings in MERS are even less clearly described and have been reported as bilateral patchy or extensive opacities [2, 12]. It has been noted that imaging features consistent with acute respiratory distress syndrome were typically identified in sicker patients [12]. The purpose of this study was to review and better describe the chest CT findings of laboratory-confirmed MERS-CoV cases.

Materials and Methods

Subjects

Approval for this study was obtained from the local research ethics committees of two hospitals; informed consent was waived. A retrospective review of the electronic archives at both hospitals was searched for all CT-imaged laboratory-confirmed MERS-CoV cases. All cases were confirmed by respiratory samples tested by real-time reverse-transcriptase-polymerase chain reaction (rRT-PCR). The rRT-PCR targeted the MERS-CoV RNA upstream region of the *E* gene and confirmed the result by targeting the open reading frame *ORF1a* and *ORF1b* regions, as previously described [13, 14]. A final cohort of seven cases was identified for our study. The available clinical, laboratory, and imaging findings were evaluated in all seven patients.

Imaging Techniques

MDCT was performed using one of the following CT scanners: 16-MDCT LightSpeed (GE Healthcare), 64-MDCT Discovery 750 HD (GE Healthcare), 64-MDCT Sensation (Siemens Healthcare), or second-generation dual-source 128-MDCT Somatom Definition Flash (Siemens Healthcare). The protocol used was as follows: end inspiratory acquisition, 100–120 kV, 200–500 mAs, 1–2.25 mm slice thickness, and 1–1.25 mm slice interval. Only one patient received 60 mL IV of iodinated contrast material (iobitridol 350 [350 mg I/mL], Xenetix, Guerbet).

Image Analysis

Two fellowship-trained thoracic radiologists, with 5 and 11 years of experience, reviewed the CT studies independently and resolved discrepancies by consensus. Images were analyzed on one of two PACS workstations: IDS7 (Sectra) and Centricity Web (GE Healthcare). The images were viewed on both lung (width, 1500 HU; level, –700 HU) and mediastinal (width, 350 HU; level, 40 HU) settings. The two readers analyzed the axial CT images but were free to evaluate the multiplanar reformats.

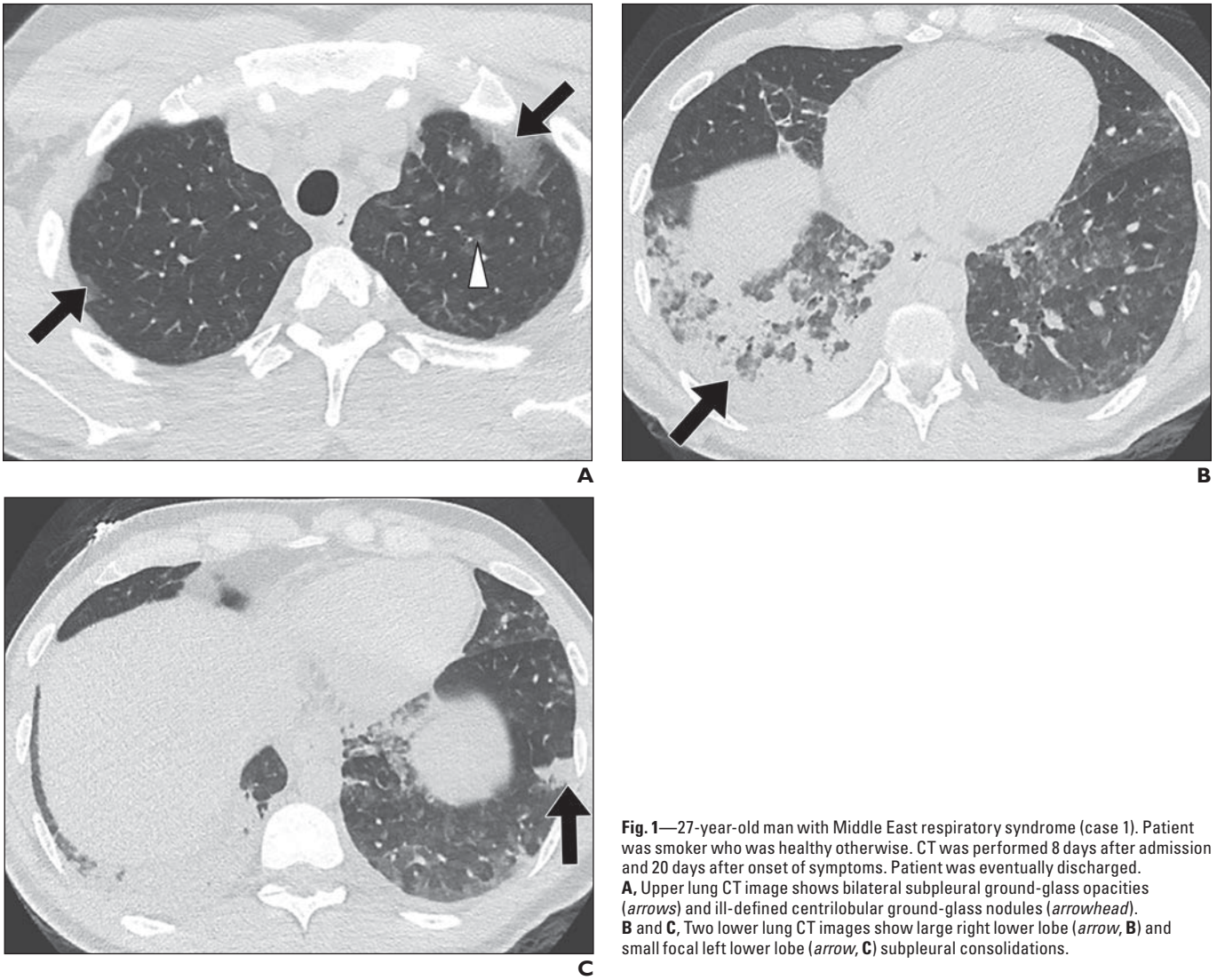

Fig. 1—27-year-old man with Middle East respiratory syndrome (case 1). Patient was smoker who was healthy otherwise. CT was performed 8 days after admission and 20 days after onset of symptoms. Patient was eventually discharged.
A, Upper lung CT image shows bilateral subpleural ground-glass opacities (*arrows*) and ill-defined centrilobular ground-glass nodules (*arrowhead*).
B and **C**, Two lower lung CT images show large right lower lobe (*arrow*, **B**) and small focal left lower lobe (*arrow*, **C**) subpleural consolidations.

The CT scans were assessed for the presence of ground-glass opacities, consolidation, cavitation, centrilobular nodules, tree-in-bud pattern, septal thickening, perilobular opacities, reticulation, architectural distortion, subpleural bands, traction bronchiectasis, bronchial wall thickening, intrathoracic lymph node enlargement, and pleural effusions. Ground-glass opacity was defined as increased lung density with no obscuration of the underlying lung markings. Consolidation was defined as increased lung density with obscuration of the underlying lung markings. Perilobular opacities were defined as polygonal or curvilinear bands bordering the secondary pulmonary lobule. Reticulation was defined as interlobular or intralobular irregular septal thickening. Subpleural bands were defined as thin linear opacities peripheral and parallel to the pleura. Traction bronchiectasis was defined as irregular or distorted dilated airways seen in areas of fibrosis.

The abnormalities were characterized as unilateral or bilateral. The distribution was categorized as focal, multifocal, or diffuse. Focal was defined as a single focus of abnormality, multifocal as more than one focus, and diffuse as involvement of most of the volume of one lung. The craniocaudal distribution of the abnormalities was categorized as upper lung predominant, lower lung predominant, or no craniocaudal predilection. The transverse distribution of the abnormalities was categorized as central (i.e., peribronchovascular), peripheral (i.e., subpleural), or no transverse predilection.

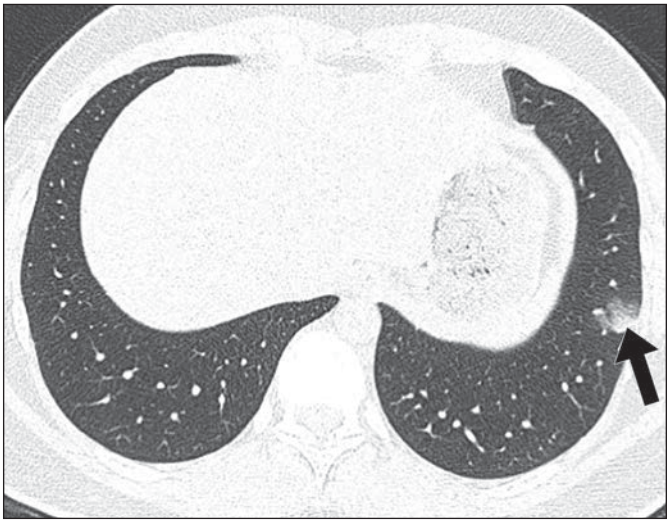

Fig. 2—19-year-old man with Middle East respiratory syndrome (case 2). CT was performed on day of admission, which was 4 days from onset of symptoms. Patient was eventually discharged. Chest CT image shows isolated focal subpleural left lower lobe consolidation (*arrow*).

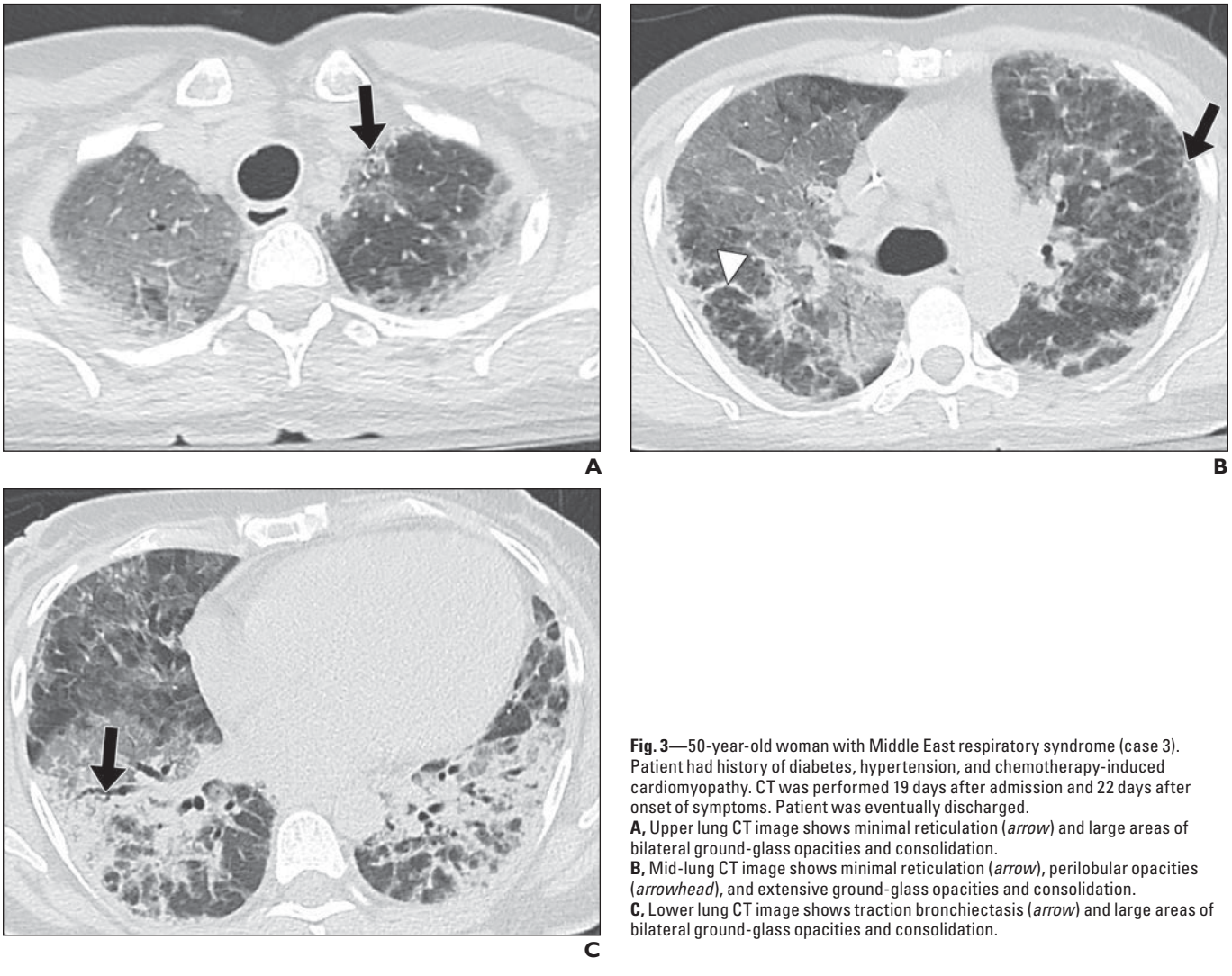

Fig. 3—50-year-old woman with Middle East respiratory syndrome (case 3). Patient had history of diabetes, hypertension, and chemotherapy-induced cardiomyopathy. CT was performed 19 days after admission and 22 days after onset of symptoms. Patient was eventually discharged.
A, Upper lung CT image shows minimal reticulation (*arrow*) and large areas of bilateral ground-glass opacities and consolidation.
B, Mid-lung CT image shows minimal reticulation (*arrow*), perilobular opacities (*arrowhead*), and extensive ground-glass opacities and consolidation.
C, Lower lung CT image shows traction bronchiectasis (*arrow*) and large areas of bilateral ground-glass opacities and consolidation.

TABLE 1: Summary of Clinical and CT Features in Seven Patients with Middle East Respiratory Syndrome Coronavirus

Patient No.	Age (y)	Sex	Habits and Comorbidities	Main Symptoms	Time From Onset to CT (d)	Main CT Findings	Distribution of CT Findings	Clinical Outcome
1	27	M	Smoking, no comorbidities	Myalgia, lethargy, back pain, abdominal pain, fever, cough	20	GGO more than consolidation, bronchial wall thickening, ill-defined centrilobular opacities, septal thickening, pleural effusions	Bilateral, peribronchovascular, predominantly subpleural and basilar	Recovered
2	19	M	None	Fever, cough	4	Consolidation	Unilateral, subpleural, focal to left lower lobe	Recovered
3	50	F	Diabetes mellitus, hypertension, chemotherapy-induced cardiomyopathy, treated lymphoma	Fever, cough, dyspnea, sputum production	22	GGO more than consolidation, perilobular opacities, septal thickening, reticulation, traction bronchiectasis	Bilateral, diffuse with no specific predominance	Recovered
4	44	M	None	Fever, cough, dyspnea	9	GGO more than consolidation, septal thickening, pleural effusions	Bilateral, peribronchovascular, predominantly subpleural and basilar	Died
5	73	M	Smoking, diabetes mellitus, hypertension, dyslipidemia	Cough, sputum production, dyspnea	4	Consolidation more than GGO	Bilateral, peribronchovascular, predominantly subpleural and basilar	Died
6	53	F	Obesity, prior resection of parotid adenoid cystic carcinoma	Fever, cough, sputum production	49	GGO, subpleural bands, architectural distortion	Bilateral, diffuse with no specific predominance	Recovered
7	83	M	Diabetes mellitus, hypertension	Fever, cough, dyspnea	9	GGO more than consolidation, pleural effusions	Bilateral, peribronchovascular, predominantly subpleural and basilar	Died

Note—GGO= ground-glass opacities.

Results

Subjects

Our group of patients consisted of seven patients, five men and two women, with an age range of 19–83 years (median age, 50 years). The time from the onset of symptoms to hospital presentation ranged from 2 to 14 days (median, 7 days). The main presenting symptoms were cough ($n = 7$), fever ($n = 6$), dyspnea ($n = 4$), sputum production ($n = 3$), abdominal pain ($n = 1$), back pain ($n = 1$), lethargy ($n = 1$), and myalgia ($n = 1$). In one patient, lethargy and myalgia preceded the respiratory symptoms by 3 days. The remaining six patients had respiratory symptoms from the onset of the infection. Only one patient had a history of contact with camels. Another patient was a physician who worked in a hospital where several proven MERS cases were being treated. The remaining five patients had no history of contact with proven MERS-CoV cases or animals. Two of the seven patients were smokers. Three of the seven patients had no significant medical history. The remaining four patients had one or more of the following comorbidities: hypertension ($n = 3$), diabetes ($n = 3$), dyslipidemia ($n = 1$), obesity ($n = 1$), and chemotherapy-induced cardiomyopathy ($n = 1$). Additionally, one patient had been treated for lymphoma and another patient had undergone resection of parotid adenoid cystic carcinoma.

Nasopharyngeal swab testing yielded a diagnosis of MERS-CoV in six of the seven patients. One of the seven patients had a false-negative swab result. Bronchoalveolar lavage (BAL) was performed in five of the seven patients, with all BAL samples testing positive for MERS-CoV. All seven patients had lymphopenia (absolute lymphocyte count $< 1.5 \times 10^3$/uL) on presentation or during hospitalization. Three patients had leukopenia (absolute white blood count, $< 4.5 \times 10^3$/uL), and three patients had thrombocytopenia (absolute platelet count $< 150 \times 10^3$/uL) on presentation or during hospitalization. The creatinine was normal on admission and became elevated (levels > 115 umol/L) during hospitalization in all seven patients. Serum LDH values were available and elevated in three of the seven patients (levels exceeding 190 U/L). AST values were elevated in all seven patients (levels > 37 U/L). ALT values were available and normal in six of the seven patients. Creatine kinase values were available and elevated in three of the seven patients (levels > 232 IU/L). Blood and sputum cultures revealed no superadded organisms in all seven patients during the entire course of hospitalization.

All patients were transferred to the ICU from the emergency department and were placed in airborne infection isolation rooms. All seven patients were started on oseltamivir (Tamiflu, Roche Laboratories) and various broad-spectrum antibiotics on admission or during hospitalization. One of the seven patients received empirical low-dose steroids during the ICU stay. Four of the seven patients survived the ICU stay, were transferred to the medical floor, and were eventually discharged. The duration of hospitalization ranged from 15 to 58 days (median duration, 31 days).

Image Analysis

One of the seven patients underwent CT on the day of admission. The remaining six patients underwent CT 1–35 days after admission (median, 11 days). The time from symptom onset to performing the CT ranged from 4 to 49 days (median, 17 days). No CT examinations were repeated during hospitalization or after discharge from the hospital.

Airspace opacities were more common than interstitial changes on the CT studies of

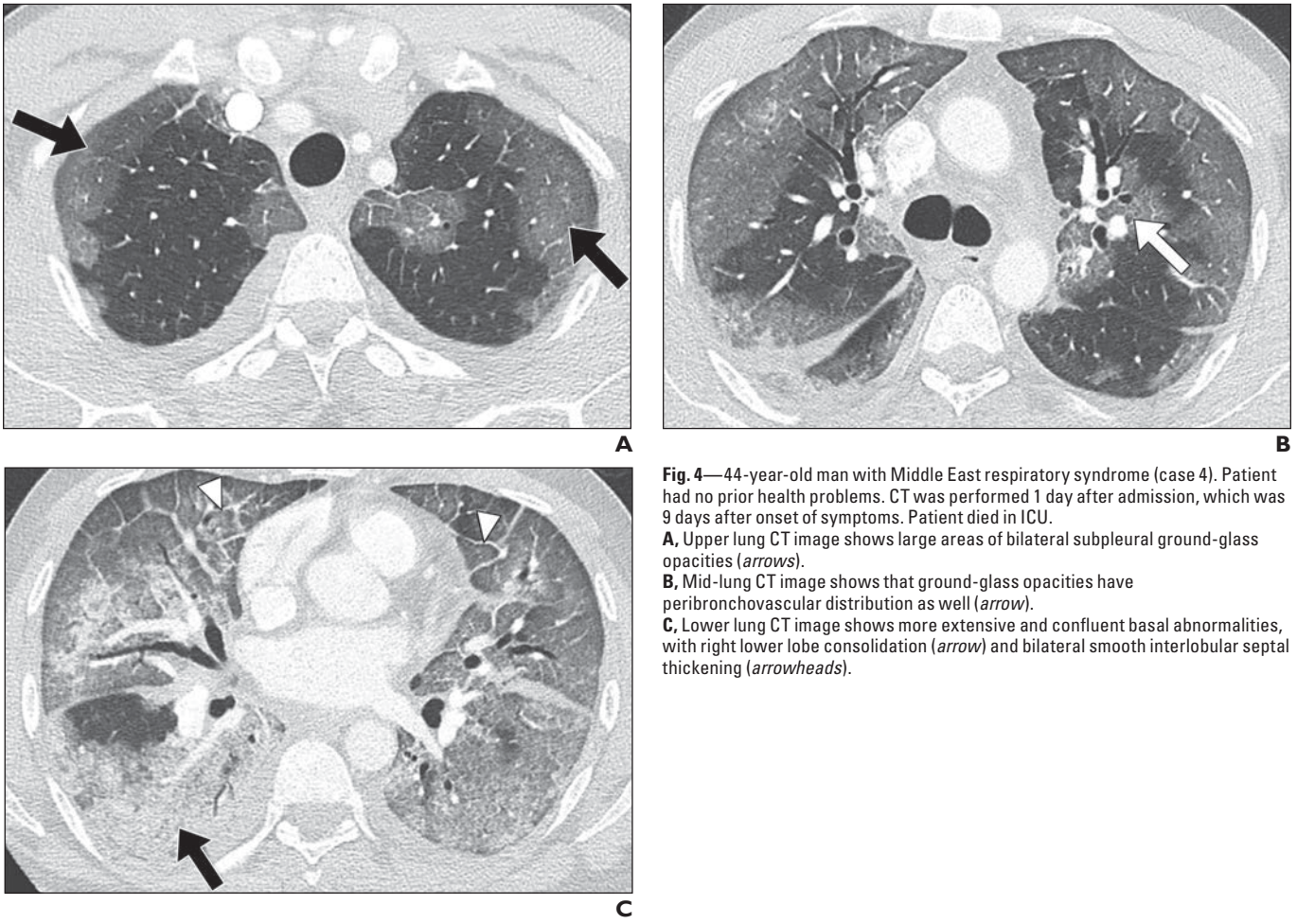

Fig. 4—44-year-old man with Middle East respiratory syndrome (case 4). Patient had no prior health problems. CT was performed 1 day after admission, which was 9 days after onset of symptoms. Patient died in ICU.
A, Upper lung CT image shows large areas of bilateral subpleural ground-glass opacities (*arrows*).
B, Mid-lung CT image shows that ground-glass opacities have peribronchovascular distribution as well (*arrow*).
C, Lower lung CT image shows more extensive and confluent basal abnormalities, with right lower lobe consolidation (*arrow*) and bilateral smooth interlobular septal thickening (*arrowheads*).

our seven patients (Table 1). Five of the seven patients had both ground-glass opacities and consolidation (Fig. 1). In those five patients, ground-glass opacities were more extensive than consolidation, with the exception of one patient. One of the seven patients had isolated ground-glass opacities and another had isolated consolidation (Fig. 2). In a patient with isolated ground-glass opacities, CT was performed 49 days after the onset of symptoms, and minimal subpleural bands and architectural distortion were present. Smooth septal thickening was identified in three of the seven patients. Minimal peripheral reticulation, traction bronchiectasis, and perilobular opacities were noted in only one patient, who underwent CT 22 days after the onset of symptoms (Fig. 3). Only one patient had both mild bronchial wall thickening and ill-defined centrilobular ground-glass nodules, suggestive of small airways involvement. Small bilateral pleural effusions were present in three of the seven patients. None of the patients had tree-in-bud pattern, cavitation, or intrathoracic lymph node enlargement.

The abnormalities were bilateral in six and unilateral in one of seven patients. The patient with unilateral involvement had a single focal consolidation in the left lower lobe. Both subpleural and lower lung–predominant airspace involvement were identified in five of the seven patients. In the remaining two patients, the abnormalities were extensive and diffuse, with no clear craniocaudal or transverse predominance. In four of five patients with subpleural predominant airspace involvement, variable degrees of peribronchovascular airspace involvement were also present (Fig. 4).

Discussion

This study shows that airspace opacities on CT are common in patients hospitalized with MERS-CoV infection. In most of our patients, ground-glass opacities were more extensive than consolidation. However, one patient had more pronounced consolidation and another had an isolated focal consolidation in the left lower lobe. Another observation is that a few patients may show septal thickening and pleural effusions. Importantly, tree-in-bud pattern, cavitation, and lymph node enlargement were not seen in our cohort.

The presence of variable degrees of lung opacities in MERS has been described in a few studies, without clearly addressing the exact distribution [2, 12]. Because our study evaluated the CT findings in this laboratory-confirmed group of MERS patients, we had the ability to better characterize the nature and distribution of the abnormalities. The predominance of airspace opacities in the subpleural and basilar lung regions is a noteworthy finding. Additionally, a few patients showed peribronchovascular involvement as well. Airspace opacities in such a distribution have been described as suggestive of an organizing pneumonia pattern [15, 16]. This pattern is reminiscent of what has been described in cases of H1N1 influenza A virus (formerly known as swine-origin influenza virus) infection, in which an imaging picture of organizing pneumonia developed in acutely sick patients [17, 18]. Although the presence of organizing pneumonia in cases of H1N1 influenza A infection was initially described in the radiology literature [17, 18], subsequent histopathology studies confirmed this pattern on evaluated lung specimens [19, 20]. It is early at this stage to reach any solid conclusions, but our understanding of MERS-CoV may undergo the same evolution as that of H1N1 influenza A virus.

In the two patients in whom the time from the onset of symptoms to performing CT was the longest (22 and 49 days), reticulation and traction bronchiectasis were seen in one patient, whereas subpleural bands and architectural distortion were seen in the other. Organizing pneumonia, a nonspecific inflammatory lung response to insults, is known to progress to a fibrotic process in some patients on longer-term follow-up [21]. Fibrotic changes after organizing pneumonia may have occurred in those two patients, but the lack of CT early in the course of the disease is a limitation to this assumption.

The WHO recommends various droplet, airborne, and contact precautions when dealing with suspected cases of MERS-CoV infection [4]. However, for several reasons, timely identification of MERS patients is not always straightforward. First, patients may present with mild or unusual symptoms [2, 4, 12]. Second, apparently healthy patients could carry MERS-CoV that may be unrecognized [22]. Third, rRT-PCR testing of initial respiratory samples may yield false-negative results [12]. Fourth, even in patients correctly identified with MERS-CoV, the result of rRT-PCR may take 24–48 hours to be processed. Thus, in patients with acute respiratory symptoms who are living in or traveling from areas of the MERS-CoV outbreak, familiarity with suggestive imaging findings may help with early isolation and management.

We acknowledge that the retrospective design and small number of patients limit our study. With this in mind, it would be difficult to reach generalized conclusions regarding how CT findings would correlate with clinical outcomes. Additionally, the time from symptom onset to performing the CT examination was variable, which limited our ability to ascertain the relationship between symptom duration and lung imaging findings. We suggest that MERS-CoV induces an organizing pneumonia lung reaction, but we had no histopathologic lung specimen correlation to solidify this observation.

In summary, the most common CT finding in hospitalized patients with MERS-CoV infection is that of bilateral, predominantly subpleural and basilar airspace changes, with more extensive ground-glass opacities than consolidation. The predilection of the abnormalities to the subpleural and peribronchovascular regions is suggestive of an organizing pneumonia pattern. Recognizing this pattern in acutely ill patients living in or traveling from endemic areas may help in the early diagnosis of MERS-CoV infection.

References

1. Zaki AM, van Boheemen S, Bestebroer TM, Osterhaus AD, Fouchier RA. Isolation of a novel coronavirus from a man with pneumonia in Saudi Arabia. *N Engl J Med* 2012; 367:1814–1820
2. Assiri A, Al-Tawfiq JA, Al-Rabeeah AA, et al. Epidemiological, demographic, and clinical characteristics of 47 cases of Middle East respiratory syndrome coronavirus disease from Saudi Arabia: a descriptive study. *Lancet Inf Dis* 2013; 13:752–761
3. World Health Organization website. Middle East respiratory syndrome coronavirus (MERS-CoV) summary and literature update—as of 27 March 2014. www.who.int/csr/disease/coronavirus_infections/MERS_CoV_Update_27_March_2014.pdf?ua=1. Accessed April 17, 2014
4. World Health Organization website. Global alert and response: Middle East respiratory syndrome coronavirus (MERS-CoV)—April 14, 2014 update. www.who.int/csr/don/2014_04_14_mers/en/index.html. Accessed April 17, 2014
5. World Health Organization website. Middle East respiratory syndrome coronavirus (MERS-CoV) summary and literature update—as of 9 May 2014. www.who.int/csr/disease/coronavirus_infections/MERS_CoV_Update_27_March_2014.pdf?ua=1. Accessed May 13, 2014
6. Memish ZA, Zumla AI, Al-Hakeem RF, Al-Rabeeah AA, Stephens GM. Family cluster of Middle East respiratory syndrome coronavirus infections. *N Engl J Med* 2013; 368:2487–2494
7. Assiri A, McGeer A, Perl TM, et al. Hospital outbreak of Middle East respiratory syndrome coronavirus. *N Engl J Med* 2013; 369:407–416
8. Memish ZA, Cotten M, Meyer B, et al. Human infection with MERS coronavirus after exposure to infected camels, Saudi Arabia, 2013. *Emerg Infect Dis* 2014; 20:1012–1015
9. Alagaili AN, Briese T, Mishra N, et al. Middle East respiratory syndrome coronavirus infection in dromedary camels in Saudi Arabia. *MBio* 2014; 5:e00884-14
10. Memish ZA, Mishra N, Olival KJ, et al. Middle East respiratory syndrome coronavirus in bats, Saudi Arabia. *Emerg Infect Dis* 2013; 19:1819–1823
11. Abdel-Moneim AS. Middle East respiratory syndrome coronazvirus (MERS-CoV): evidence and speculations. *Arch Virol* [Epub 2014 Feb 11]
12. Arabi YM, Arifi AA, Balkhy HH, et al. Clinical course and outcomes of critically ill patients with Middle East respiratory syndrome coronavirus infection. *Ann Intern Med* 2014; 160:389–397
13. Corman VM, Eckerle I, Bleicker T, et al. Detection of a novel human coronavirus by real-time reverse-transcription polymerase chain reaction. *Euro Surveill* 2012; 17:20285
14. Corman VM, Müller MA, Costabel U, et al. Assays for laboratory confirmation of novel human coronavirus (hCoV-EMC) infections. *Euro Surveill* 2012; 17:20334
15. Ujita M, Renzoni EA, Veeraraghavan S, Wells AU, Hansell DM. Organizing pneumonia: perilobular pattern at thin-section CT. *Radiology* 2004; 232:757–761
16. Travis WD, Costabel U, Hansell DM, et al. An official American Thoracic Society/European Respiratory Society statement: update of the international multidisciplinary classification of the idiopathic interstitial pneumonias. *Am J Respir Crit Care Med* 2013; 188:733–748
17. Ajlan AM, Quiney B, Nicolaou S, Müller NL. Swine-origin influenza A (H1N1) viral infection: radiographic and CT findings. *AJR* 2009; 193:1494–1499
18. Ajlan AM, Khashoggi K, Nicolaou S, Müller NL. CT utilization in the prospective diagnosis of a case of swine-origin influenza A (H1N1) viral infection. *J Radiol Case Rep.* 2010; 4:24–30
19. Gill JR, Sheng ZM, Ely SF, et al. Pulmonary pathologic findings of fatal 2009 pandemic influenza A/H1N1 viral infections. *Arch Pathol Lab Med* 2010; 134:235–243
20. Marchiori E, Zanetti G, Fontes C, Santos M, Influenza A (H1N1) virus-associated pneumonia: high-resolution computed tomography—pathologic correlation. *Eur J Radiol* 2011; 80:e500–e504
21. Kligerman SJ, Franks TJ, Galvin JR. From the radiologic pathology archives: organization and fibrosis as a response to lung injury in diffuse alveolar damage, organizing pneumonia, and acute fibrinous and organizing pneumonia. *RadioGraphics* 2013; 33:1951–1975
22. World Health Organization website. Global alert and response: Middle East respiratory syndrome coronavirus (MERS-CoV)—June 26, 2013 update. www.who.int/csr/don/2013_06_26/en/index.html. Accessed April 17, 2014